# Modeling of 3D Field Patterns of Downtilted Antennas and Their Impact on Cellular Systems

L. Thiele, T. Wirth, K. Börner, M. Olbrich and V. Jungnickel
Fraunhofer Institute for Telecommunications
Heinrich-Hertz-Institut
Einsteinufer 37, 10587 Berlin, Germany
{thiele, thomas.wirth, jungnickel}@hhi.fraunhofer.de

J. Rumold and S. Fritze
KATHREIN-Werke KG,
Anton-Kathrein-Strasse 1-3, 83004 Rosenheim, Germany
{juergen.rumold, stefan.fritze}@kathrein.de

***Abstract*—Advanced multi-antenna techniques, such as multi-user MIMO (MU-MIMO) and cooperative transmission are known to increase system performance in cellular deployments. However, it is well known that cellular systems suffer from multi-cell interference. Antenna downtilt is a common method used to adjust interference conditions especially in urban scenarios with a high base station density. Performance evaluation is generally based on multi-cell simulations using 2D models, neglecting the elevation component of the base station antennas. In this work we concentrate on 3D antenna models based on real world antennas with high directivity, their approximation and impact on cellular systems.**

## I. Introduction

Recent advances valid for an isolated cell indicate huge performance gains obtained from multiple-input multiple-output (MIMO) communications [1], [2]. However, cellular systems still suffer from multi-cell interference. In order to develop advanced multi-antenna techniques, such as multi-user MIMO (MU-MIMO) [3] or cooperative transmission [4], we have to ensure a realistic modeling of multi-cell interference. Thus, we are able to investigate their performance more realistically. Performance evaluation is commonly based on multi-cell simulations using 2D models as e.g. 3GPP's extended spatial channel model (SCME) or WINNER Phase I model (WIM1). The WINNER Phase II model (WIM2), which was released recently [5], is capable of using 3D antenna geometries and field patterns.

In this work we concentrate on 3D antenna models based on real world antennas from KATHREIN, their approximation and impact on cellular systems. The goal is to provide appropriate antenna approximations, which can easily be included in channel models like the SCME used for performance evaluation of cellular MIMO communications. In general, 2D field patterns for the azimuth ($\phi$) and elevation ($\theta$) dimensions are available for various antenna types. Fig. 1 depicts these field patterns for the KATHREIN 80010541 antenna, which is one of the standard antennas used for future 3G Long Term Evolution (3G-LTE) sectorized cellular urban deployments. This antenna has an azimuth pattern with full width at half maximum (FWHM) of $\phi_{\text{FWHM}} = 60°$ and an elevation pattern with $\theta_{\text{FWHM}} = 6.1°$. The electrical downtilt angle $\alpha = \theta'_t - 90°$ is adjustable. For 3D approximation, we will use these 2D

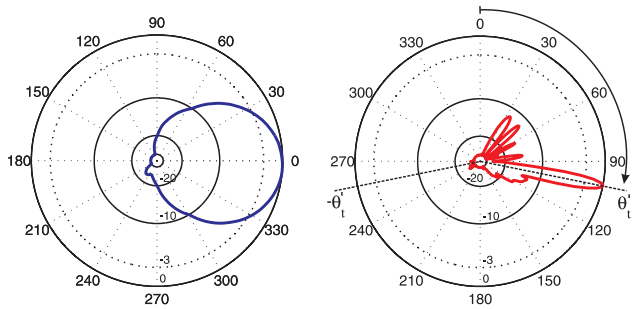


(a) Azimuth; $\phi_{\text{FWHM}} = 60°$. (b) Elevation; $\theta_{\text{FWHM}} = 6.1°, \alpha = 7°$

Fig. 1. Radiation patterns from KATHREIN 80010541 antenna and 2.6 GHz carrier frequency

radiation patterns. In the following we compare two simple approximation techniques, their approximation errors and impact on cellular systems with respect to user geometries obtained from system level simulations.

## II. Approximation of 3D antenna radiation patterns

Common 3D antenna approximation approaches based on 2D field patterns are known from literature [6]–[8]. In this work we focus on the two most promising approaches, suitable for the approximation of highly directive antennas: a conventional method and a novel technique described in [8]. Fig. 2(a) depicts a 3D measured antenna diagram from KATHREIN 80010541 antenna in the phi-theta plane with a downtilt angle $\alpha = 10°$.

### A. Conventional method

A simple way to create a quasi 3D pattern is to combine azimuth and elevation field patterns by adding their gains in both directions with equal weights.

$$G(\phi, \theta) = G_H(\phi) + G_V(\theta) \tag{1}$$

Using this method we obtain a 3D pattern which is symmetrical in $\phi$ direction. This method lacks in appropriate modeling at the back side of the antenna, i.e. between $-90° \leq \phi \leq 90°$. These directional gains at the backside of the antenna would be very small unlike those in a real antenna. Fig. 2(b) depicts the

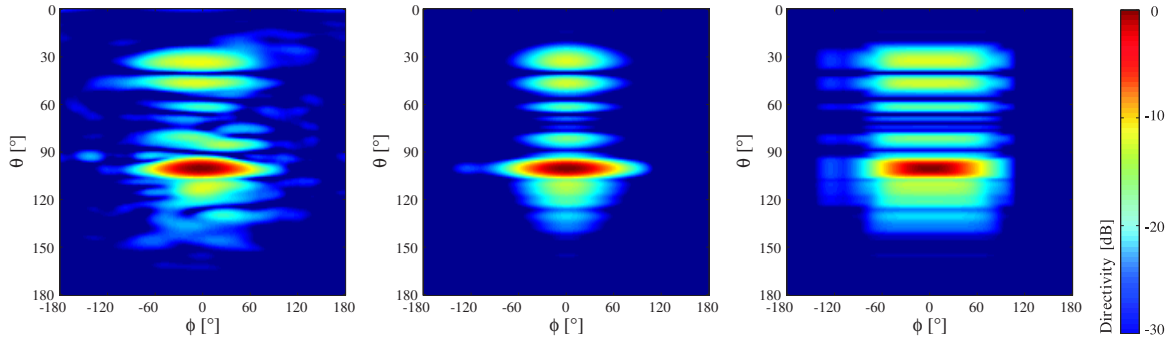


(a) measured pattern (b) conventional method (c) novel technique

Fig. 2. Antenna patterns shown in the phi-theta plane. The attenuations are limited to 30 dB. The tilt angle is fixed to $\alpha = 10°$

resulting approximation in phi-theta-plane, where the overall dynamics are limited to 30 dB. It may be observed that the main lobe's shape is pretty close to the one obtained from the measured antenna radiation pattern. The components for $-60° \leq \phi \leq 60°$, which lie outside the 120°-sector, are suppressed for all side lobes in vertical dimension. However, their gain is 20 dB below the maximum. Thus, we expect these components to be less important for antennas with high directivity.

### B. Novel technique

Another approximation method we consider in this work was proposed by [8], which we will refer to as *novel technique*. The difference to the conventional method is that the elevation and azimuth gains are both weighted to extrapolate the spatial gain

$$G(\phi,\theta) = \underbrace{\frac{\omega_1}{\sqrt[k]{\omega_1^k+\omega_2^k}}}_{A_1} G_H(\phi) + \underbrace{\frac{\omega_2}{\sqrt[k]{\omega_1^k+\omega_2^k}}}_{A_2} G_V(\theta) \quad (2)$$

$$\begin{aligned} \omega_1(\phi,\theta) &= vert(\theta)\cdot[1-hor(\phi)] \\ \omega_2(\phi,\theta) &= hor(\phi)\cdot[1-vert(\theta)] \end{aligned}$$

The weighting functions $\omega_1$ and $\omega_2$ are based on linear values $hor(\phi)$ and $vert(\theta)$ of the antenna gains in azimuth and elevation direction, respectively. $k$ is a normalization-related parameter which referring to [8] provides best results for $k = 2$. Both $A_1$ and $A_2$ are smaller than one since $vert(\theta)$ and $hor(\phi)$ vary between zero and one.

The enumerators $\omega_n$ of $A_n$ control the weight of elevation and azimuth pattern, respectively. For small gains in the azimuth direction, the antenna gains in the elevation pattern are reduced in their magnitude and vice versa. Thus, gain factors are more restricted in their range compared to (1). Further, if we choose values for $\theta$ where the elevation pattern has its maximum, i.e. $vert(\theta) = 1$, results in $\omega_2 = 0$. Hence, only the azimuth pattern is weighted according to $(1 - hor(\phi))$. In general, the lower the gain, the smaller the weight. Fig. 2(c) depicts the resulting approximation based on [8] in the phi-theta-plane. Comparing the resulting radiation pattern with the one in Fig. 2(b) shows a higher spread in power distribution among the phi-theta-plane. This property is closer to the measured pattern. However, the deformation in the main lobe seems to be more significant, which is not comparable with the measured pattern. Thus, we expect results obtained from the conventional approximation to be closer to reality. Due to that reason we mainly limit our investigations to the conventional method.

## III. Effects in an Isolated Cell

As a starting point for our investigations we focus on the effects, which may be observed in an isolated cell. Therefore, we consider a channel with non line of sight (NLOS) propagation conditions in an urban-macro scenario. Thus, the path loss equation according to [9] is given by

$$\begin{aligned} \mathrm{PL_{dB}} &= 40(1-4\cdot10^{-3}\Delta h_{BS})\,log_{10}(d) \\ &\quad -18\,log_{10}(\Delta h_{BS}) + 21\,log_{10}(f_c) + 80, \end{aligned} \quad (3)$$

where $d$ [km] is the distance between base station (BS) and mobile terminal (MT); $f_c$ [MHz] is the carrier frequency and $\Delta h_{BS}$ [m] is the BS height measured from the average rooftop level. Setting $f_c = 2.6$ GHz and $\Delta h_{BS} = 15$ m yields

$$\mathrm{PL_{dB}} = 130.5 + 37.6\log_{10}(d) \quad (4)$$

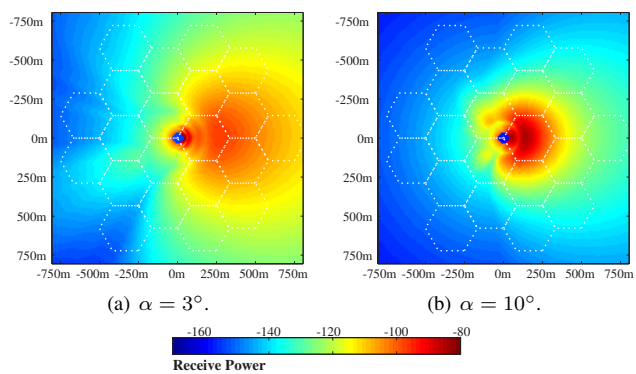


(a) $\alpha = 3°$. (b) $\alpha = 10°$.

Fig. 3. Gains for the directive antenna in addition to an urban path loss for different downtilt angles

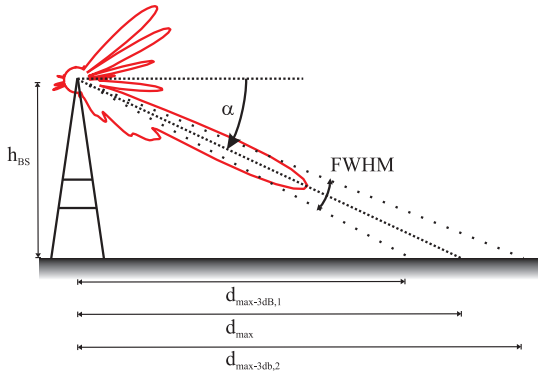


Fig. 4. Base station setup with downtilted antenna

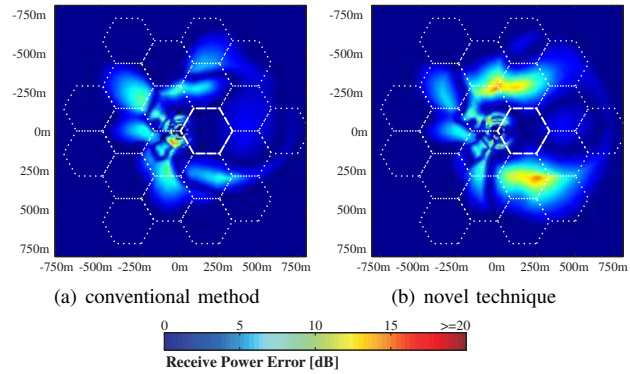


Fig. 5. Path loss plus directional gain errors in relation to the measured pattern plus path loss at 2.6 GHz

In combination with the directive antenna gains obtained from a given 3D antenna diagram, we estimate the received power as a function of the distance between BS and position of the MT. Fig. 3 depicts the antenna gains for the directive antenna in addition to an urban path loss from (3), both seen at height of the terminal antenna and for different tilt angles. Hexagonal sectors are shown as white dotted lines with an inter-site distance (ISD) of 500 m. The BS antenna is located at the point [0,0] at $h_{BS} = 32$ m above ground level, i.e. the average rooftop height is assumed to be 17 m. It may be observed that in case of a downtilt angle $\alpha = 3°$ the sector antenna is serving up to 3 neighboring sectors with equivalent power as available in its own sector. In this application $\alpha = 10°$ seems to meet requirements of a cellular system with an ISD of 500 m best: high gain level in own sectors and low values for neighboring cells. This is also verified by (5) indicating the effective cell radius, i.e. the distance where main lobe and ground level intersect, refer to Fig. 4. The distance range covering the FWHM area can be determined to 129 m $\leq d \leq$ 244 m, assuming $\alpha = 10°$.

$$d_{max} = \frac{h_{BS}}{\tan\alpha} \quad (5)$$

$$d_{max-3\,\mathrm{dB}} = \frac{h_{BS}}{\tan\left(\alpha \pm 0.5\,\theta_{\mathrm{FWHM}}\right)} \quad (6)$$

In the following, we focus on the quality of both approximation methods from (1) and (2). For comparison we use the distance dependent received power based on the measured radiation pattern combined with the urban path loss from (4). Fig. 5 shows the differential received power maps for the conventional and novel approximation for $\alpha = 10°$, respectively. The conventional method, depicted in Fig. 5(a), shows superior precision over the approximation based on [8], depicted in Fig. 5(b), both described in sections II-A and II-B.

To substantiate simulation results obtained for an isolated cell, we include outdoor measurement results from the city area of Berlin. These measurements were carried out in the campus area of Technical University Berlin (TUB) with an average rooftop height of approx. 30m. The BS antenna (KATHREIN 80010541) was fixed at $h_{BS} = 32$ m with a

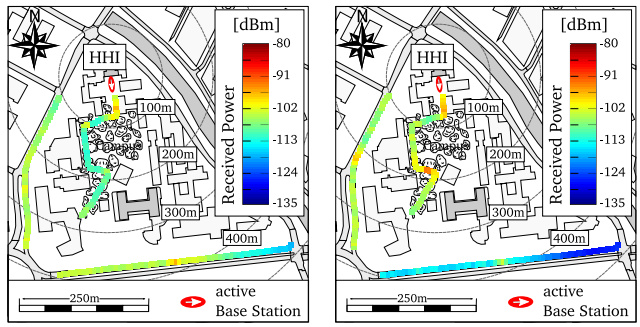


(a) 3° downtilt (b) 10° downtilt

Fig. 6. Measured path loss at $1W$ transmission power and $h_{BS} = 32$ m

variable tilt angle, which was set to $\alpha = \{3°, 10°\}$. Figs. 6(a) and 6(b) show the received power for the given tilt angle. For $\alpha = 3°$ the BS antenna serves the whole area with approx. $-100$ dBm. Otherwise, for $\alpha = 10°$ the campus area and the outer region are both served with $-90$ dBm and $-110$ dBm, respectively. In particular, close to the BS there is gain of 10 dB. In general, we observe equivalent behavior as already found in Figs. 3(a) and 3(b): the smaller the tilt angle $\alpha$ the larger the area, which is served with equivalent, but lower received power. On the other hand with higher tilt angles, the BS focuses its transmit power to a smaller area.

## IV. Effects in a Cellular System

In the next section we turn our focus to the downtilted antenna and its effects observable in a cellular environment, i.e. effects on the neighboring cells. Therefore we consider a center cell surrounded by one tier of triple-sectorized cells. Each sector is served by single antenna with $h_{BS} = 32$ m, where all tilt angles are set to identical values. Thus, all BSs are assumed to cover a region of equivalent size. Fig. 7 indicates achievable signal to interference ratio (SIR) conditions in such a setup under the assumption of $\alpha = \{3°, 10°\}$. Again we employ the urban path loss model from (4) in combination with the radiation pattern obtained from the conventionally approximated antenna pattern (1). Since the evaluation scenario is limited to 7 cells, only the highlighted

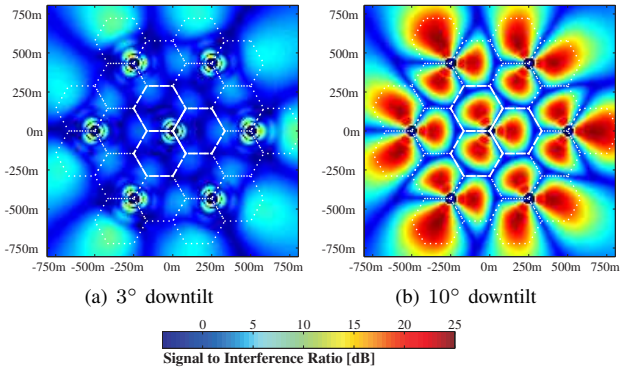


Fig. 7. SIR maps obtained from simplified multi-cell simulations

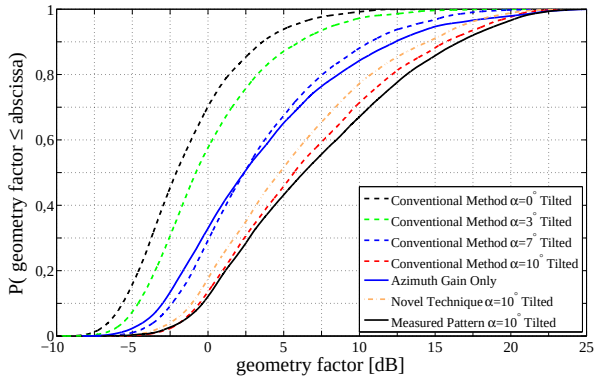


Fig. 8. User geometries obtained from multi-cell SCME simulations

TABLE I
SIMULATION ASSUMPTIONS

| parameter | value |
|---|---|
| channel model | 3GPP SCME |
| scenario | urban-macro |
| $f_c$ | 2.6 GHz |
| frequency reuse | 1 |
| signal bandwidth | 18 MHz, 100 RBs |
| intersite distance | 500m |
| transmit power | 46 dBm |
| sectorization | triple, with FWHM of 68° |
| elevation pattern | with FWHM of 6.1° |
| BS height $h_{BS}$ | 32m |
| MT height | 2m |

center cell reflect reasonable SIR values. For small $\alpha$, SIRs inside these 3 sectors are limited to an average value of 0 dB, refer to Fig. 7(a). In contrast, for $\alpha = 10°$ the achievable SIRs cover a range from 0 dB at the cell edge and up to 25 dB in the cell center, refer to Fig. 7(b). This result indicates that a tilt angle in the order of $\alpha = 10°$ is favorable for a generic cellular system with an ISD of 500 m and $h_{BS} = 32$ m. However, in real scenarios where BSs are not placed in a symmetric grid, $\alpha$ would be chosen according to the desired coverage area, i.e. cell size.

## V. System Level Simulations using SCME

In the following we investigate the effects from modeling 3D antenna radiation patterns in a triple-sectored hexagonal cellular network with 19 BSs in total. This refers to the commonly used simulation assumption [10], i.e. a center cell surrounded by two tiers of interfering cells. The MTs are placed in the center cell and are always served by the BS whose signal is received with highest average power over the entire frequency band. In this way, BS signals transmitted from 1st and 2nd tier model the inter-cell interference. Simulation parameters are given in Table I. The SCME [11] with urban macro scenario parameters is used, yielding an equivalent user's geometry as reported in [12].

*User geometries:* Fig. 8 compares the resulting user geometries obtained from both approximation methods (1) and (2), while assuming $\alpha = 10°$. For validation we include the geometry factor distribution obtained from simulations using the measured radiation pattern from Fig. 2(a), where $\alpha = 10°$. The geometry from the conventional method is close to the cumulative distribution function (CDF) based on the measured pattern, while the CDF which is based on the novel approximation technique shows a significant gap. Hence, the choice of the approximation method influences simulation results considerably. Further, we show changes on the geometry factor due to the downtilt angle, which is selected from $\alpha = \{0°, 3°, 7°, 10°\}$ based on the conventional antenna approximation (dashed lines). Comparing these results with the user geometries obtained from simulations which consider 2D antenna modeling only, shows equivalent values for $\alpha = 7°$. For smaller downtilt angles we observe user geometries which are significantly below the well known values for the 2D case.

*Top-N power distribution:* Consider the application of a cellular radio system consisting of $\mathcal{K}$ BSs operating in the downlink direction. It is reasonable to assume that a MT located in a specific cell of that network is able to detect a subset of $N = |\mathcal{N}|$ strongest BS signals, i.e. a set of BSs $\mathcal{N} \subset \mathcal{K}$ of all BSs within the deployment. Based on the user-specific channels to all BSs, a so-called Top-$N$ power distribution is generated by instantaneously sorting the estimated power distributions. These sorted received powers are put into one overall statistic, enabling us to observe the power distributions for all channels seen by a MT. At two given sample points, the strongest signals may be related to different sectors or sites and are included in the same CDF, referred to as top-1. The power distributions of the 1st to the 10th strongest channels are given in Fig. 9. We observe that power distributions are broadened due to large downtilt angles $\alpha$. Intuitively spoken, cells become more separated, i.e. signal conditions with strong interference are mitigated directly at the physical layer (PHY layer).

Finally, we determine the source of the four strongest signals received at the MT. Fig. 10 depicts the histogram showing the probabilities for the source, i.e. center cell, 1st tier and 2nd tier, of the four strongest signals in the cellular scenario. These results are obtained from simulations using the azimuth

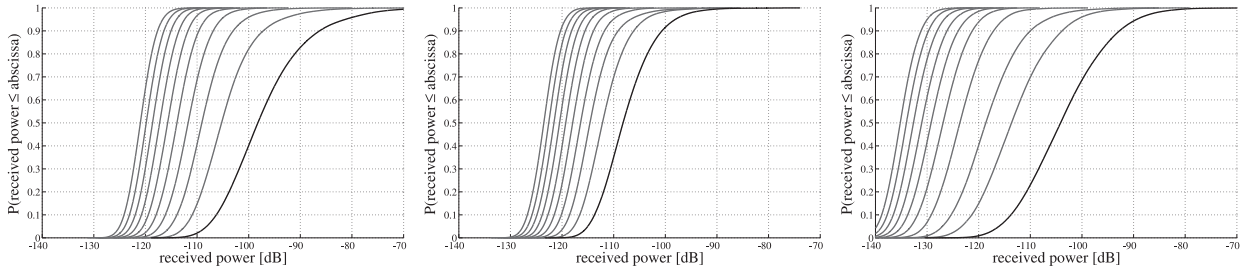


(a) azimuth pattern only (2D) (b) conventional method $\alpha = 3°$ (c) conventional method $\alpha = 10°$

Fig. 9. Power distributions for the 10 strongest signals

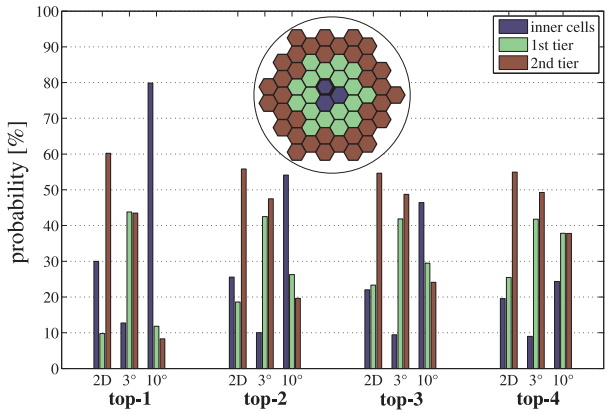


Fig. 10. Source of the four strongest signals, obtained from simulations considering azimuth pattern (2D) only, as well as 3D conventionally approximated antennas with $\alpha = \{3°, 10°\}$

pattern only, i.e the standard 2D assumption. Further, results are compared with probabilities using the conventional antenna approximation with downtilt angles $\alpha = \{3°, 10°\}$. Concentrating on the strongest signal, i.e. top-1, and comparing these probabilities, we can observe two main differences: for the 2D simulation the origin for top-1 signal lies with 60% in the 2nd tier and with 30% in the inner cell. With $\alpha = 10°$ the situation is changed. The top-1 signal has its origin with 80% in the inner cell and with less than 10% in the 2nd tier. For completeness note that for $\alpha = 10°$ signals are more likely to have their origin close to the terminal position.

## VI. Conclusion

In this work we compared two simple 3D antenna approximation methods and focused on antenna types, typically used in 3G-LTE sectorized urban deployments. These methods use 2D radiation patterns for approximation, which are generally provided by antenna manufacturers. The simple conventional method for 3D antenna approximation provides results close to those obtained by using a 3D measured radiation pattern. Simulation and measurement results further showed significant SIR gains from downtilted BS antennas in cellular deployments. Finally, the results point out that full 3D antenna modeling is necessary to evaluate advanced multi-antenna techniques, like MU-MIMO and cooperative transmission. Especially, the evaluation of joint downlink transmission comparing dynamic versus fixed BS clustering will benefit from this work.

## Acknowledgements

The authors are grateful for financial support from the German Ministry of Education and Research (BMBF) in the national collaborative project EASY-C under contract No. 01BU0631.

## References

[1] G. Foschini and M. Gans, "On limits of wireless communications in a fading environment when using multiple antennas," *Wireless Personal Communications*, no. 3, pp. 311–335, 1998.

[2] L. Zheng and D. Tse, "Diversity and multiplexing: A fundamental tradeoff between in multiple antenna channels," *IEEE Transactions on Information Theory*, vol. 49, no. 5, pp. 1073–1096, May 2003.

[3] D. Gesbert, M. Kountouris, R. Heath, C.-B. Chae, and T. Salzer, "Shifting the MIMO paradigm," *IEEE Signal Processing Magazine*, vol. 24, no. 5, pp. 36–46, Sept. 2007.

[4] F. Boccardi and H. Huang, "A near-optimum technique using linear precoding for the MIMO broadcast channel," *Acoustics, Speech and Signal Processing, 2007. ICASSP 2007. IEEE International Conference on*, vol. 3, pp. III–17–III–20, April 2007.

[5] L. Hentil, P. Kysti, M. Kske, M. Narandzic, and M. Alatossava, "MATLAB implementation of the WINNER Phase II Channel Model ver1.1," Tech. Rep., Dec. 2007. [Online]. Available: https://www.ist-winner.org/phase_2_model.html

[6] W. Araujo Lopes, G. Glionna, and M. de Alencar, "Generation of 3d radiation patterns: a geometrical approach," in *Vehicular Technology Conference, 2002. VTC Spring 2002. IEEE 55th*, vol. 2, 2002, pp. 741–744 vol.2.

[7] F. Gil, A. Claro, J. Ferreira, C. Pardelinha, and L. Correia, "A 3d interpolation method for base-station-antenna radiation patterns," *Antennas and Propagation Magazine, IEEE*, vol. 43, no. 2, pp. 132–137, Apr 2001.

[8] T. Vasiliadis, A. Dimitriou, and G. Sergiadis, "A novel technique for the approximation of 3-d antenna radiation patterns," *Antennas and Propagation, IEEE Transactions on*, vol. 53, no. 7, pp. 2212–2219, 2005.

[9] TR 101 112 v3.2.0, "Universal Mobile Telecommunications System (UMTS); Selection procedures for the choice of radio transmission technologies of the UMTS," Apr. 1998.

[10] L. Thiele, M. Schellmann, T. Wirth, and V. Jungnickel, "Cooperative multi-user MIMO based on reduced feedback in downlink OFDM systems," in *42nd Asilomar Conference on Signals, Systems and Computers*. Monterey, USA: IEEE, Nov. 2008.

[11] 3GPP TR 25.996 V7.0.0, "Spatial channel model for multiple input multiple output (MIMO) simulations (release 7)," July 2007. [Online]. Available: http://www.tkk.fi/Units/Radio/scm/

[12] H. Huang, S. Venkatesan, A. Kogiantis, and N. Sharma, "Increasing the peak data rate of 3G downlink packet data systems using multiple antennas," vol. 1, april 2003, pp. 311–315 vol.1.